Hindawi
Journal of Chemistry
Volume 2018, Article ID 6982014, 14 pages
https://doi.org/10.1155/2018/6982014

Research Article

Adsorptive Removal of Methylene Blue and Crystal Violet onto Micro-Mesoporous Zr_3O/Activated Carbon Composite: A Joint Experimental and Statistical Modeling Considerations

H. Ait Ahsaine,[1] Z. Anfar,[1] M. Zbair,[2] M. Ezahri,[1] and N. El Alem[1]

[1]*Materials and Environment Laboratory, Department of Chemistry, Ibn Zohr University, Agadir, Morocco*
[2]*Catalysis and Materials Corrosion Laboratory, Department of Chemistry, Chouaib Doukkali University, El Jadida, Morocco*

Correspondence should be addressed to H. Ait Ahsaine; a.hassan@uiz.ac.ma

Received 25 July 2018; Revised 9 September 2018; Accepted 24 September 2018; Published 1 November 2018

Academic Editor: Luqman C. Abdullah

Zirconium oxide/activated carbon (Zr_3O/AC) composite was synthesized to remove methylene blue (MB) and crystal violet (CV) from the aqueous medium. The Zr_3O/AC sample was characterized by X-ray diffraction (XRD), scanning electron microscopy (SEM), energy dispersive X-ray analyses (EDS), Raman spectroscopy (RS), BET surface area, and Fourier transform infrared spectroscopy (FTIR). XRD profiles confirmed the successful synthesis of the zirconium oxide/activated carbon composite. SEM images showed multideveloped walls with irregular particle size with channel arrays. The nitrogen physisorption combines I and IV types with a calculated BET surface area of 1095 m^2/g. Raman spectrum illustrated a disorder of both crystalline structure and the graphitic structure. The adsorption was better fitted to the pseudo-second-order (PSO) kinetic model. Langmuir model fitted better the experimental results of MB adsorption, whereas the CV was better consistent with the Freundlich model. The obtained results suggested that the MB and CV adsorption might be influenced by the mass transfer that involves multiple diffusion steps. The maximum adsorption capacities are 208.33 and 204.12 mg/g for MB and CV, respectively. The MB and CV removal mechanisms were proposed, and statistical optimization was performed using central composite design combined with the response surface methodology.

1. Introduction

Nowadays, many industrial activities such as coloring, textile, cosmetic, paper, food, paint, printing, and pharmaceuticals are considered a big concern from the environmental point of view as many hazardous synthetic dyes are generally produced [1]. These pollutants are regarded as reactive, acid, and basic and are very harmful to environment including vegetation, humans, and animals [2]. Methylene blue (MB) is a common basic dye that is used for dyeing clothes in textile industries [3]. MB can cause the adverse effects such as cyanosis, vomiting, diarrhea, tachycardia, and jaundice on human beings. [3, 4]. Crystal violet is another type of toxic pollutant with a poor degradability that is widely used in textile industries because of its low cost and high solubility in water [5, 6].

Various processes are effectively investigated for the removal and elimination of pollutants like chemical precipitation, adsorption, membrane filtration, biological treatment, and photocatalytic degradation [7, 8]. Among these techniques, adsorption is the most effective and broadly utilized approach due to its many advantages being not only the relatively low cost and ease implementation of the operation process [9] but also the effectiveness of the adsorption process that primarily depends on the performance of the adsorbent mass transfer and thermodynamics. Nevertheless, traditional adsorbents including carbonaceous materials, metal nanoparticle oxides, and polymer resins suffer from either low adsorption capacities or low efficiency [10–16]. Therefore, in the general framework of environmental and waste management, there is a need to synthesize environmental recyclable and friendly materials with better

uptake and thermodynamic and kinetic properties. Recently, ZrO_2 or zirconium-based composites was used as an adsorbent in the gas and liquid phase. More precisely, zirconia ZrO_2 was used for CO_2 adsorption and hydrogen adsorption to understand the relation to the dehydrogenation of hexane [17, 18]. While in recent works, zirconium and zirconia was used with activated carbon (AC) as composites for the removal of pollutants in water. For instance, Mullick and Neogi [19] have impregnated zirconium on powdered activated carbon (AC) using ultrasound as the tool for synthesis and applying it for fluoride adsorption from water. However, Xiong et al. [20] have used iron-zirconium-modified activated carbon nanofiber for the adsorption of phosphates. Similar works have used these types of composite for the removal of other pollutants [21, 22].

In the present work, commercial suboxide Zr_3O nanoparticles have been fixed onto AC to improve the sorption capacity of MB and CV dyes. This suboxide is unique because of close-packed Zr layers in H stacking and O in octahedral voids, and additionally, the OZr_6 octahedra share vertices to form a 3D framework. This 3D framework is very beneficial if it is fixed within the prepared adsorbent leading to high density interactions. The effect of various parameters such as mass loading of Zr_3O/AC, pH, contact time, dye concentration, temperature, and regeneration was studied. In addition, the mechanism of MB and CV onto Zr_3O/AC and adsorptions experiments optimization were investigated using FTIR analysis after adsorption and RSM-CCD method. It should be noted that the optimization of the adsorption system using classic adsorption and experimental protocol based on changing each single variable does not give useful information about variables. Hence, RSM coupled with the CCD method was considered as a new approach and helpful allowing changing more than a variable at one time and studying the interaction effects between operational parameters [8, 23–29].

To the best of our knowledge, this work reports an effective methodology to study the adsorption of CV and MB, a straightforward study to calculate the optimum parameters through surface modeling, and a sorption mechanism based on different techniques before and after adsorption.

2. Materials and Methods

2.1. Synthesis of the Activated Carbon. The chemicals used in this study were of analytical reagent grade and used without purification. The activated carbon-based almond shell was prepared by chemical activation using KOH. For this purpose, the almond shell was mixed with KOH solution (Sigma-Aldrich, 98%), 10 g of KOH (Sigma-Aldrich, 90%), with 20 g of almond shell and 100 mL of distillated water to obtain a solution which was heated at 60°C for 12 h and then dried at 110°C. Then, the dried sample was pyrolyzed under N_2 flow (200 cm^3/min) at 300°C for 2 h and then at 800°C for 3 h at a heating rate of 10°C/min. The Zr_3O/AC composite was prepared by impregnation of 20 wt.% of zirconium oxynitrate $ZrO(NO_3)_2{\cdot}xH_2O$ (Sigma-Aldrich, 99%) on the prepared activated carbon after 6 hours of stirring at room temperature. Finally, the impregnated almond shell was dried at 70°C for 12 h and then pyrolyzed at 800°C for 1 hour.

2.2. Adsorption Experiments. The adsorption batch system tests were conducted in glass beakers (150 mL) containing 50 mL of CV or MB solutions with a constant stirring rate. Then, the influence of different key parameters was fully investigated. After a certain time, the pollutants concentration was determined using a UV-Vis spectrophotometer (UV 2300) at their respective maximum wavelengths of 664 nm for MB and 582 nm for CV. The adsorbed amount and removal percentage at different conditions were calculated using the following equations:

$$Q_{\text{ads}} = (C_0 - C_e) * \frac{V}{m}\ (\text{mg/g}),$$
$$\%\ \text{removal} = \left(\frac{(C_0 - C_e)}{C_0}\right) * 100, \quad (1)$$

where C_0 (mg/L) and C_e (mg/L) are the initial and equilibrium liquid-phase concentrations, m (g) is the mass of Zr_3O/activated carbon, and V (L) is the volume of the MB/CV solution.

Langmuir [30] and Freundlich [31] were used to analyze the equilibrium data, and the adsorption isotherm models were also applied to simulate information about the distribution of adsorbate molecules at the solid-liquid interface. Table 1 summarizes the mathematical parameters of these models. However, the equations of the selected kinetics models to fit the experimental data are listed in Table 2.

3. Results and Discussion

3.1. Structural and Textural Characterizations. Figure 1 shows the XRD patterns of the synthesized zirconia-AC powder, and the diffractogram shows two aspects: amorphous aspect in the range of 20–30° and amorphous aspect in the range of 40–50°, which are characteristics to carbon/two-dimensional reflections of turbostratic layer stacks [32] and to graphitic structure of activated carbon. The intense diffraction profiles are associated with the crystalline hexagonal zirconium oxide Zr_3O (JCPDS card no 03-065-7450), the calculated lattice parameters for zirconia by Le Bail fit are $a = b = 5.613$ (2) and $c = 5.192$ (3), and these parameters are very close to the standard Zr_3O JCPDS zirconia file.

Thermal analyses, illustrated in Figure 1(b), show the thermal decomposition of zirconia/AC composite as a function of temperature. This experiment was performed under air. Two major weight losses were recorded: the first loss of 15% below 100°C is attributed to the surface-adsorbed H_2O [33], while the second weight loss of 60% in the range of 300–480°C might be originated from thermal decomposition organic matters such as lignin, cellulose, and hemicelluloses of the almond shell. An intense endothermic peak was recorded for this loss showing the remarkable amount of decomposed products [34].

Figure 2 illustrates the morphology and elemental dispersive spectroscopy of Zr_3O/AC composite. In the SEM

Table 1: Isotherm models.

Isotherm	Equation	Description
Langmuir	$1/Q_e = 1/Q_m + 1/(K_L Q_m C_e)$	C_e: concentration at equilibrium; Q_e = uptake at equilibrium; Q_m = maximum adsorption capacity; K_L= energy of adsorption
Freundlich	$\ln(Q_e) = \ln K_F + 1/n \ln(C_e)$	K_F = adsorption capacity; n = intensity of adsorption; $1/n = 0$ irreversible; $1/n >$ unfavourable; $0 < 1$ favourable

Table 2: Kinetic models used to fit the experimental data.

Kinetic models	Equation	Description
Pseudo-first order	$\ln(Q_e - Q_t) = \log(Q_e) - K_1 t/2.303$	Q_t = uptake at time t; Q_e = uptake at equilibrium; K_1 = rate constant
Pseudo-second order	$t/Q_t = 1/(K_2 Q_t^2) + 1/Q_e$	K_2 = rate constant
Intraparticle diffusion	$Q_t = K_{di} t^{0.5} + C$	K_{di} = rate constant

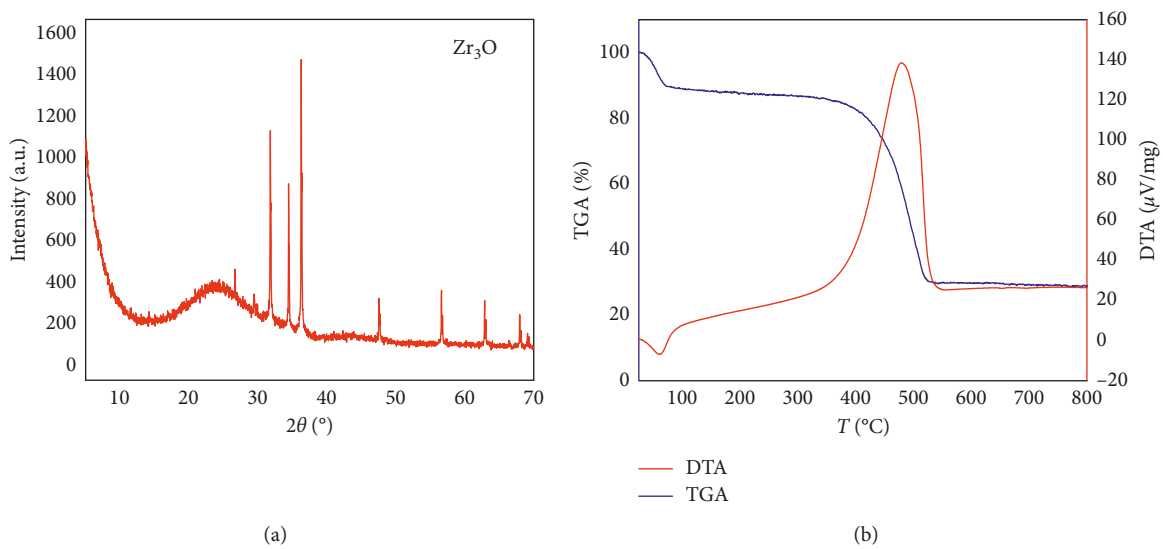

Figure 1: (a) X-Ray diffraction of Zr_3O/AC composite and (b) TGA/DTA of the Zr_3O/AC.

micrographs, multideveloped walls were observed, and pores can be seen with irregular particles and channel arrays in the range of few micrometers to few hundred micrometers. Clearly, knowing that almond shell contains micropores, it is inferred that the AC preserved the original structure of the almond after even after carbonization. The results of elemental analysis indicate the presence of three main atoms: carbon, oxygen, and zirconium.

Raman analysis is a very important tool for the characterization of active modes in the activated carbons adsorbents [35, 36]. Clearly, all the samples have two obvious D and G bands, which are assigned to the chaos and disorder of the crystalline structure and the graphitic structure of carbon materials, respectively [37, 38]. The synthesized Zr_3O/AC and AC were studied by Raman analysis, and the results are presented in Figure 3(a). The spectra displayed the typical spectra of AC with the characteristic D and G bands at 1362 and 1604 cm^{-1}, respectively. Furthermore, the intensity of Zr_3O/AC decreased indicating that the preparation process of Zr_3O/AC slightly changed the structure of activated carbon. Moreover, this means that the degree of graphitization of Zr_3O/AC decreases because zirconia occupies the pore channel [39].

The N_2 physisorption isotherm is illustrated in Figure 3(b). It combines types I and IV characteristics, meaning the coexistence of microporous and mesoporous structures in AC and Zr_3O/AC. Indeed, the distributions of pores size confirm the presence of micropores and mesopores in AC and Zr_3O/AC, and pore size distributions shown in Figure 3(c) are bimodal with a peak at around 0.5 nm for microporous structures and around 2 nm for mesoporous structures. The Zr_3O/AC BET surface area is 1095 m^2/g with total pore volume of 0.66 cm^3/g (0.16 cm^3/g of microporous volume and 0.56 cm^3/g of mesoporous volume).

The FTIR analysis of Zr_3O/AC composite is displayed in Figure 3(d). In the spectrum, a broad and strong absorption band at approximately 3449 cm^{-1} attributed to the O-H stretching vibration of water molecules adsorbed on the surface Zr_3O/AC [40]. The spectrum of Zr_3O/AC presents a peak for Zr-O stretching vibration at 620 cm^{-1} [41].

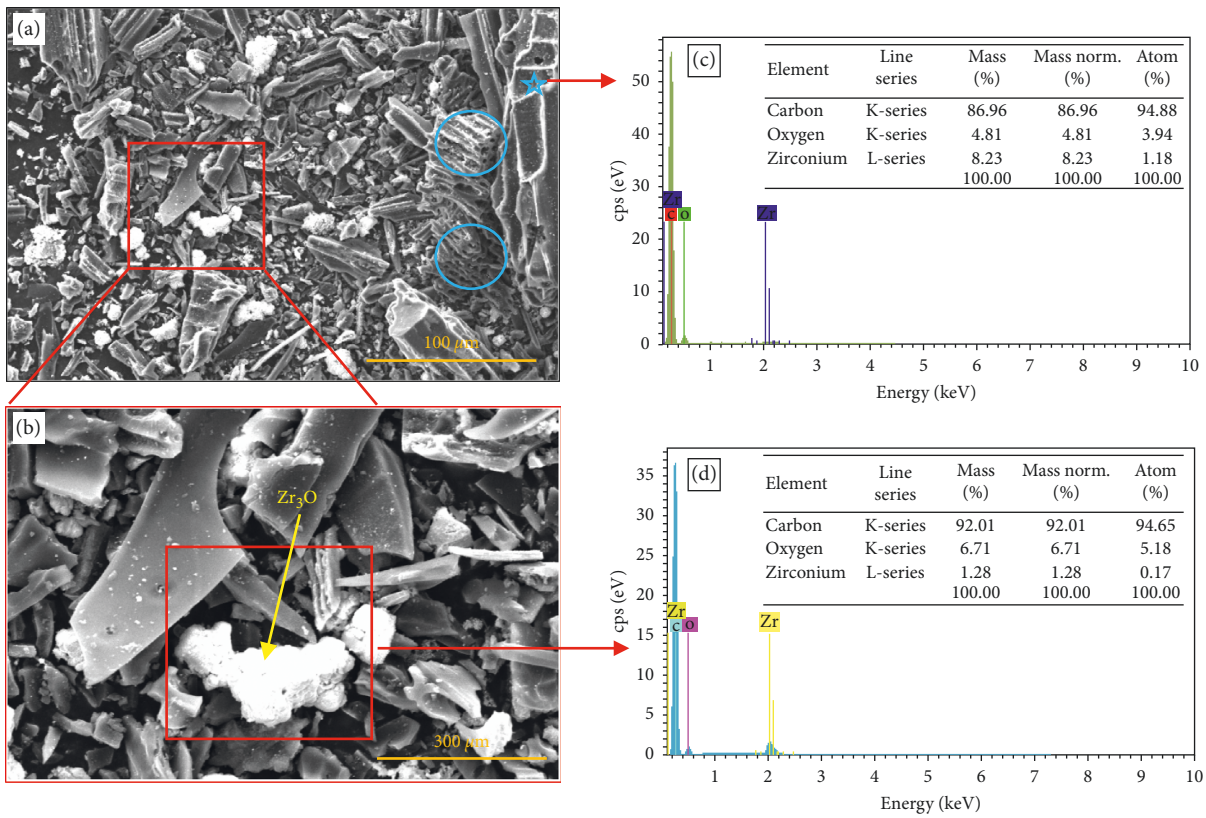

Figure 2: (a-b) SEM photographs of the Zr_3O/AC and (c-d) elemental EDS analyses.

However, the band centered on 1622 cm^{-1} indicates enhancement in the aromatic C=C groups [27, 42].

3.2. Adsorption Results

3.2.1. Influence of Operational Parameters. Binding sites and surface promoted by Zr_3O/AC doses are one of the main parameters influencing the adsorption process. Consequently, several experiments of the dyes removal with different Zr_3O/AC doses have been conducted to evaluate the effect of these key factors. These experiments have been performed at room temperature unless mentioned. The influence of Zr_3O/AC doses on MB and CV dyes removal by Zr_3O/AC is presented in Figure 4; As the Zr_3O/AC composite weight increased from 5 mg to 16 mg, the percentage removal increased as well from 84.43% to 100% for MB removal and from 75.41% to 98% for CV removal. The increase in MB and CV removal at higher dosages explain (i) the increase in number of active binding sites and (ii) bulk surface area [43].

Additionally, up to 20 mg, the dyes removal was not significantly affected by further increase in the Zr_3O/AC amount due to the possibility of aggregation, which limits the active surfaces for adsorption. The optimum Zr_3O/AC dosage was found to be 16 mg for both dyes.

Figure 5(b) illustrates the removal of MB and CV dyes as a function of solution pH. Knowing that pH can play a substantial role in the adsorbent surface charges and interfacial solid-liquid transport [44], the pH-dependence experiment has been performed for both MB and CV. As the pH increases, adsorption of both dyes on Zr_3O/AC was found to be increasing; this is mainly due to elimination of the positive proton in the aqueous media thereby promoting activities of electrostatic attraction between the positive charges of both dye and the composite Zr_3O/AC. Indeed, according to the point of zero charge (Figure 5(a)), it is confirmed that the surface of the composite can be negatively charged at pH higher than 7.5. While at an acidic pH, the functional groups of activated carbon become protonated, which are mainly the carboxylic (-COOH-), phenolic (-OH-), and chromonic group. At pH 3, the surface charge of Zr_3O/AC becomes more positively charged, which enhances MB and CV electrostatic repulsion: the number of positively charged sites on Zr_3O/AC increased and negatively charged sites on Zr_3O/AC decreased. Therefore, the electrostatic repulsion between the Zr_3O/AC sites and the positively charged CV and MB dye molecules increased which inhibit the adsorption pathway.

Figure 6 describes the influence of contact time on MB and CV adsorption by Zr_3O/AC. It was observed that the adsorption process of both dyes takes place in two different stages:

(i) The first stage was rapid which infers strong electrostatics between cationic dyes and the Zr_3O/AC positive surface.

(ii) The second stage was with no significant improvement of the adsorbed dyes, and this equilibrium

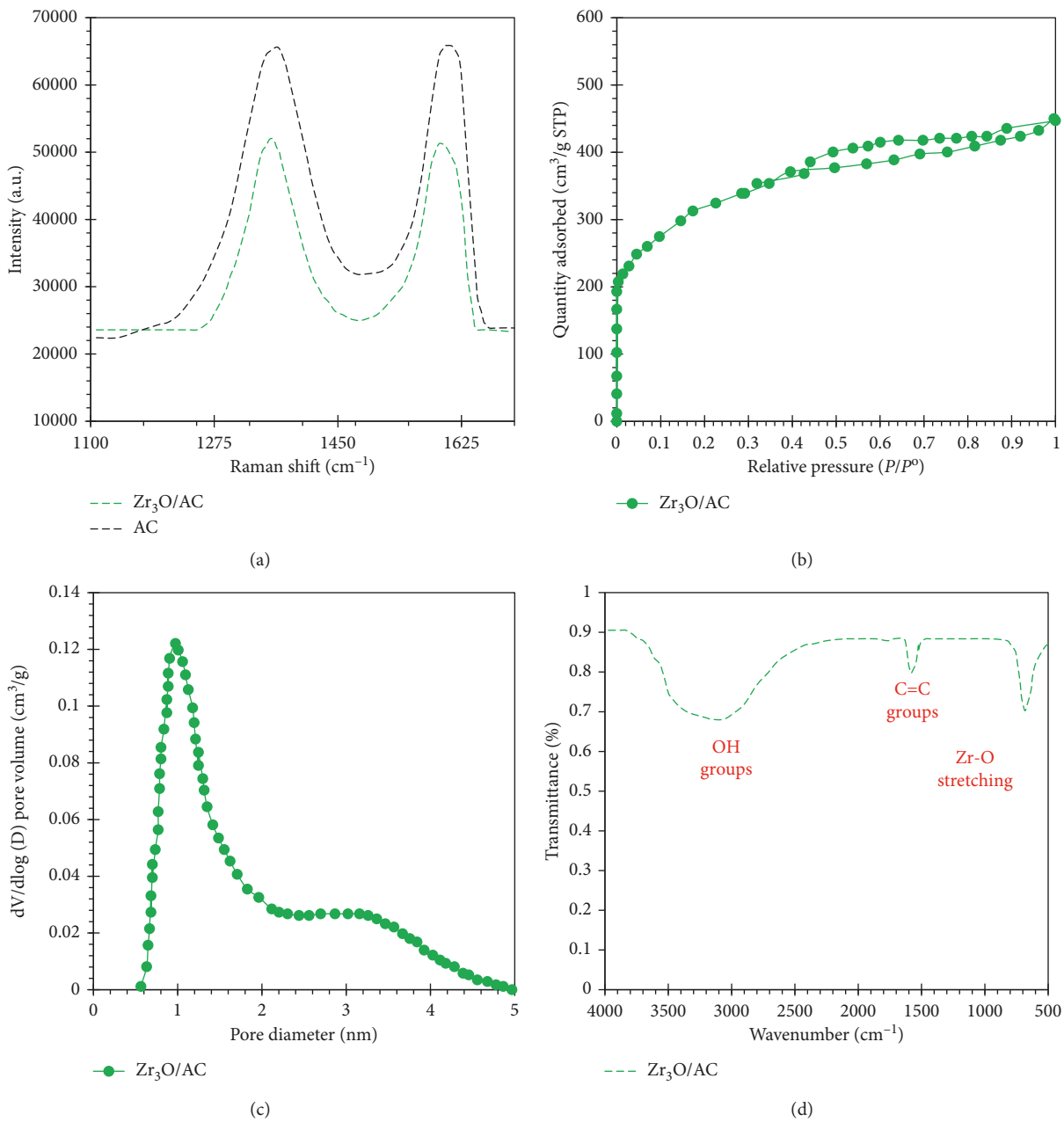

Figure 3: (a) Raman spectroscopy of the AC and Zr_3O/AC; (b) N_2 physisorption analyses; (c) pore size distribution curve; (d) FTIR spectroscopy of the Zr_3O/AC adsorbent.

stage could be due to the fast saturation of the binding sites in the Zr_3O/AC surface.

3.2.2. Kinetics and Isotherm Adsorption. In this section, pseudo-first-order (PFO), pseudo-second-order (PSO), and intraparticle diffusion (IPD) kinetic models were used to fit the experimental data of MB and CV adsorption on Zr_3O/AC. It is well established that the pseudo-first-order kinetic model has been widely applied for the adsorption of solid/liquid systems [45–47].

Table 3 lists different calculated parameters using PFO and PSO models. Figure S1 (Supporting information) shows the fitting of experimental data to the PSO model at different initial concentrations of both MB and CV dyes, and the correlation coefficient is more significant than those of the PFO model. Moreover, a large difference of Q_e between the experiment ($Q_{e,exp}$) and calculation ($Q_{e,cal}$) is observed [48]. These data support the fact that the adsorption data are well represented by the PSO kinetics model for the entire adsorption period of MB and CV dyes onto Zr_3O/AC [49].

In order to gain more insights into the kinetics of the adsorption process, the IPD model was studied. The plot (Q_t vs $t_{1/2}$) (Figure 7) shows an initial curved portion followed by a linear portion and a plateau.

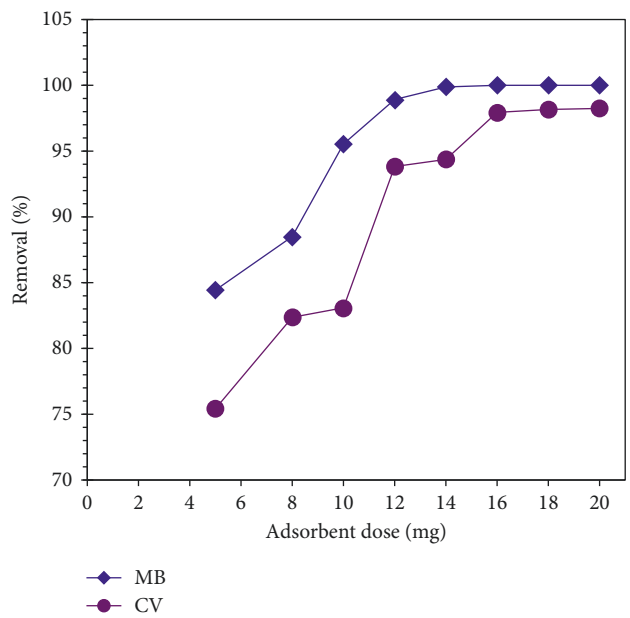

Figure 4: Effect of adsorbent dose on MB and CV dyes removal by Zr_3O/AC.

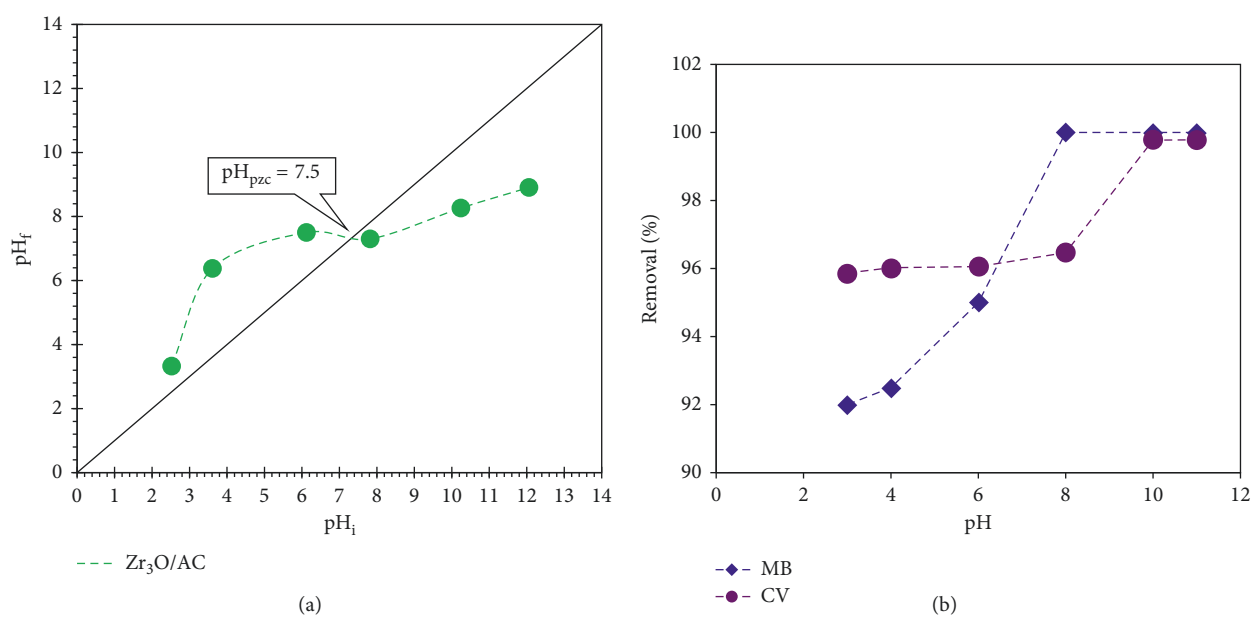

Figure 5: (a) Point of zero charge of the composite; (b) effect of initial pH solutions on MB and CV dyes removal by Zr_3O/AC.

It is clear that the adsorption processes of both MB and CV dyes can be roughly divided into three steps, as indicated by the guidelines for each portion: The first portion is attributed to the diffusion of the MB and CV molecule through solution to the external surface of the Zr_3O/AC composite. This is a fast process that mainly depends on the surface area of the Zr_3O/AC. The second portion is attributed to gradual equilibrium with IPD as the rate-determining step. The last step is due to an adsorption/desorption equilibrium which is established for both MB and CV dyes [8]. As can be seen from the Figure 7, the Zr_3O/AC exhibits faster adsorption kinetics at the initial adsorption stage due to its much higher surface area, as inferred in physisorption measurement.

The adsorption isotherm models were used to investigate the interaction between the MB and CV dyes and the Zr_3O/AC when the adsorption process reaches equilibrium. Figure S2 shows plots of adsorption data of MB and CV dyes fitted to Langmuir and Freundlich isotherm models. Table 4 summarizes the isotherm parameters for this study. It is obvious that the Langmuir model provides a better fit for MB and Freundlich models for CV. A good fit with the Langmuir model indicate monolayer adsorption. However, the Freundlich model is indicating multilayer adsorption.

We have provided an extensive comparison of Zr_3O/AC to the best performing materials reported to date in Table 5.

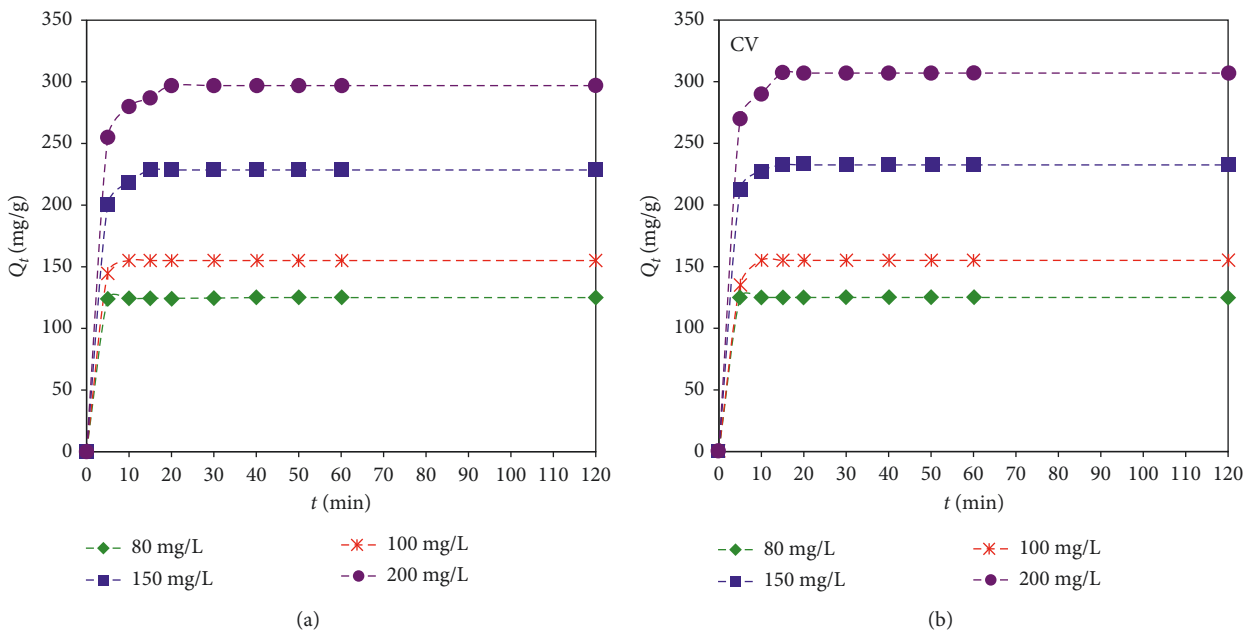

Figure 6: Effect of contact time on the removal of MB (a) and CV (b) onto Zr_3O/AC at 25°C.

Table 3: PFO and PSO fitting kinetic parameters of the experimental data.

	C_{intial} (mg/L)	$Q_{e,exp}$ (mg/g)	PFO			PSO		
			$Q_{e,cal}$ (mg/g)	K_1 (min^{-1})	R^2	$Q_{e,cal}$ (mg/g)	K_2 (g/mg·min)	R^2
MB	80	125.000	0.752	0.005	0.054	125.000	0.128	0.999
	100	155.035	1.553	0.014	0.087	156.250	0.102	0.999
	150	228.507	2.837	0.032	0.163	227.273	0.022	0.999
	200	296.937	4.871	0.046	0.234	294.118	0.010	0.999
CV	80	125.000	0.760	0.005	0.049	125.000	0.107	0.999
	100	155.078	1.774	0.018	0.087	156.250	0.046	0.999
	150	232.510	2.355	0.026	0.156	232.558	0.031	0.999
	200	307.002	3.286	0.036	0.165	312.500	0.013	0.999

Our prepared material is one of the best adsorbents for the removal of both MB and CV.

3.2.3. Regeneration of Zr_3O/AC. Reusability was carried out by regenerating Zr_3O/AC with 1% sodium hydroxide at room temperature for 3 hours. The regenerated Zr_3O/AC was then washed with Milli-Q water and dried in a vacuum oven.

The Zr_3O/AC was separated and washed with distilled water. Recycling efficiency of Zr_3O/AC was investigated for the removal of MB and CV for 3 cycles. The results show that the adsorption efficiency of Zr_3O/AC was reduced to 88% for MB and to 82% for CV dye (Figure 8). We should note that, after every cycle, NaOH was used as a desorption medium to remove adsorbed MB ions from the Zr_3O/AC surface.

3.2.4. Statistical Analysis and Model Fitting. The significance of the independent variables and their interactions was tested with various statistical analyses such as analysis of variance (ANOVA), correlation coefficient (R^2), and adjusted correlation coefficient (R^2_{adj}) [58]. The Box-Behnken matrix used in this work is presented in Table 1S. The analysis of variance results (Table 6) suggests that the developed models (Equations (2) and (3)) are highly significant with a very low P value for all models:

$$Y_{(R\%,\text{MB onto } ZrO_2-AC)} = 99.498 + 0.379X_{AD} - 0.084X_{IC} + 0.112X_{CT} - 0.304X_{AD}^2 + 0.145X_{AD}X_{IC}, \quad (2)$$

$$Y_{(R\%,\text{VC onto } ZrO_2-AC)} = 92.253 + 5.299X_{AD} - 0.686X_{IC} - 0.177X_{CT} - 3.287X_{AD}^2 + 3.058X_{IC}^2 + 2.956X_{CT}^2 + 0.555X_{AD}X_{IC}, \quad (3)$$

where X_{AD}, X_{IC}, and X_{CT} represent the adsorbent dose, initial dyes concentration, and contact time, respectively.

The R^2 values of full second-order polynomial regression models were found to be 0.951 (R^2_{adj} 0.895) and 0.972 (R^2_{adj}

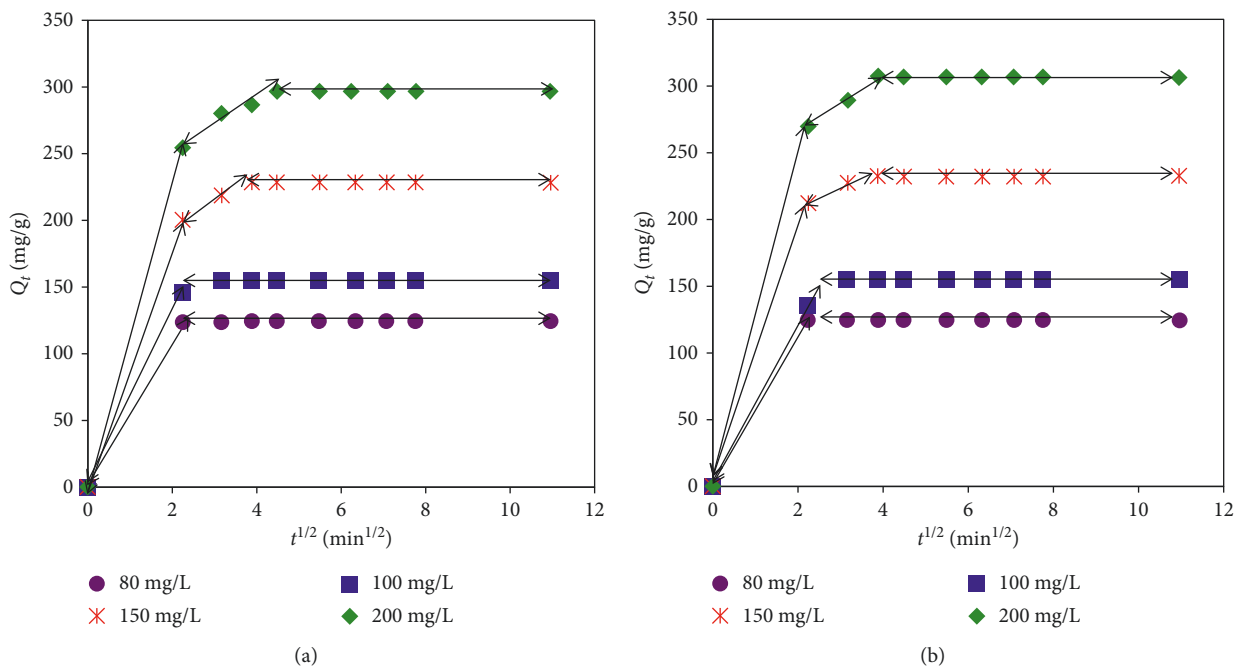

Figure 7: The plots of the intraparticle diffusion model of MB (a) and CV (b).

Table 4: Constants of Langmuir and Freundlich simulations of the MB and CV adsorption isotherms.

	Langmuir				Freundlich		
	Q_{max} (mg/g)	K_L (L·min^{-1})	R_L	R^2	K_F (mg/g)	n	R^2
MB	208.33	16.0	0.001	0.998	242.60	2.929	0.225
CV	169.49	11.80	0.001	0.492	204.12	0.910	0.915

Table 5: Comparison between different reported activated carbons and Zr_3O/AC composite.

AC adsorbent	Q_{max} (mg/g)	Ref.
MB		
Karanj fruit hull	154.8	[50]
Macadamia nut endocarp	194.70	[51]
Wood	60.97	[52]
Ficus carica bast	47.62	[53]
Sawdust	416.7	[42]
This work	208.33	—
CV		
Bamboo leaves powder	393.16	[54]
Male flowers of coconut tree	85.84	[55]
Male flowers of coconut tree	60.42	[55]
Waste apricot	57.80	[56]
Tomato plant root	94.34	[57]
This work	204.12	—

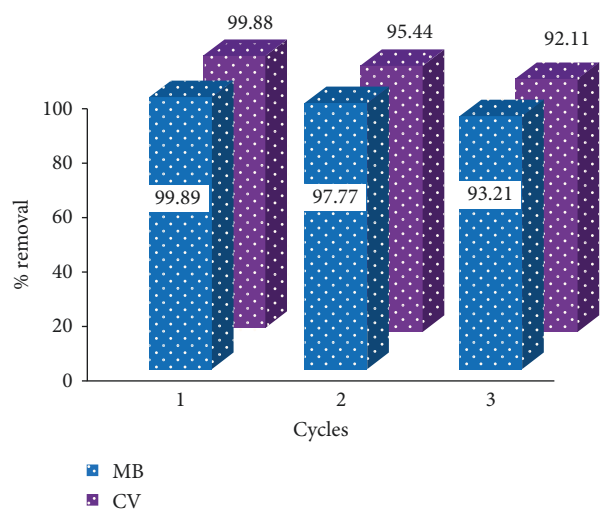

Figure 8: Regeneration efficiency of Zr_3O/AC for MB and CV removal.

0.952) for MB and CV adsorption on Zr_3O/AC, respectively [8]. Moreover, the control test was used to determine the significance of coefficients of the parameters [59]. The linear, quadratic, and interaction effects of the parameters are given in Table 7. The results confirm that most of the coefficients models were significant (P values are less than 0.05) except quadratics effects of contact time, initial concentration, and the interactions effects of CT-IC and AD-CT, which are statistically insignificant (P values are more than 0.05). The same conclusion was observed in the case of CV adsorption onto Zr_3O/AC.

3.2.5. Optimization of CV and MB Using RSM. Pareto diagrams (Figure S3) indicate the percent influence of different independent variables on MB and CV adsorption onto Zr_3O/AC. An observation of the Pareto diagram makes it possible to say that the Zr_3O/AC dose and initial

Table 6: Analysis of variance and coefficients of determination.

	Sum of squares	Degrees of freedom	Mean square	F_{obs}	P value
MB adsorption onto Zr_3O/AC					
Regression	1.8019	9	0.2002	189.4786	<0.0001
Residue	0.0933	8	0.0117		
Lack of fit	0.0880	3	0.0293	27.7681	0.00152
Error	0.0053	5	0.0011		
Total	1.8952	17			
R^2	0.951				
$R^2{}_A$	0.895				
CV adsorption onto Zr_3O/AC					
Regression	348.6312	9	38.7368	6027.5101	<0.0001
Residue	8.0777	8	1.0097		
Lack of fit	8.0455	3	2.6818	417.2990	<0.0001
Error	0.0321	5	0.0064		
Total	356.7088	17			
R^2	0.977				
$R^2{}_A$	0.952				

Table 7: Analysis of the variance-reduced model.

Source	Coefficient	t exp	P value
MB adsorption onto Zr_3O/AC			
a_0	99.498	7498	<0.0001
a_{AD}	0.379	32.96	<0.0001
a_{IC}	−0.084	−7.29	0.0007
a_{CT}	0.112	9.79	0.00018
a^2_{AD}	−0.304	−19.55	<0.0001
a^2_{IC}	0.006	0.37	0.723
a^2_{CT}	0.013	0.86	0.431
a_{AD-IC}	0.145	8.92	0.000295
a_{AD-CT}	−0.037	−2.31	0.069
a_{CT-IC}	−0.008	−0.46	0.664
CV adsorption onto Zr_3O/AC			
a_0	92.253	2819	<0.0001
a_{AD}	5.299	186.95	<0.0001
a_{IC}	−0.686	−24.21	<0.0001
a_{CT}	−0.177	−4.15	0.0089
a^2_{AD}	−3.287	−85.64	<0.0001
a^2_{IC}	3.058	79.69	<0.0001
a^2_{CT}	2.956	77.02	<0.0001
a_{AD-IC}	0.555	13.85	<0.0001
a_{AD-CT}	−0.088	−2.18	0.081
a_{CT-IC}	−0.003	−0.06	0.953

concentration factors account more than 84.81% of the variation of the response in the case of MB adsorption onto Zr_3O/AC. For the adsorption of CV onto Zr_3O/AC, the Zr_3O/AC dose and the quadratic effects of Zr_3O/AC dose, contact time, and initial concentration are the most influential parameters on the adsorption efficiency, with an influence percentage of 48.59, 18.70, 16.18, and 15.12%, respectively.

From this study, it can be clearly seen that the Zr_3O/AC dose (with a positive influence) and the initial concentration (with a negative influence) are the first factors influencing the MB and CV adsorption onto Zr_3O/AC or Zr_3O/AC. This probably returns to the availability of active sites, when the Zr_3O/AC mass of the support increases [60].

To achieve the maximum adsorption of the CV and MB dyes onto Zr_3O/AC and AC, the RSM modeling was used (Figures 9(a) and 9(b)). The optimum values of different independent variables (initial dye concentration, Zr_3O/AC dose, and contact time) are determined as shown in Table 8. It shows that the model-predicted values are in very good agreement with the experimentally determined values which confirm that the proposed model combined with RSM is an effective approach for modeling the adsorption process and to understand the relationships between the independent variables and response.

3.2.6. Adsorption Mechanism. From the FTIR, Raman, and EDS analyses, a large number of hydroxyl functional groups and carbonyl functional group on the surface of Zr_3O/AC were observed. Knowing that the prepared material has a very high surface area, the functional groups are participating in the adsorption mechanism of CV and MB as a function of solution pH and the load of Zr_3O/AC on the surface. After CV adsorption, the FTIR spectrum of the Zr_3O/AC, presented in Figure 10(a), shows characteristic changes due to the adsorption of CV onto Zr_3O/AC: the intensity of the peak representing the stretching vibrations of the O-H group shifted and the peak representing the stretching vibrations of the C-C group diminished. This might be due to the formation of chemical bonds between C-C of Zr_3O/AC and electrophilic N^+ of CV. Furthermore, the Zr-O peak shifted to higher wavenumbers suggesting a formation of chemical bonds between Zr-O and N^+ of CV dye. The same behavior was observed in the case of MB adsorption on Zr_3O/AC. As shown in the FTIR spectroscopy after MB (Figure 10(b)), -OH, C=C, and Zr-O peaks shifted to different frequencies, confirming the interaction between these groups and our MB dye. Figure 10(c) shows the proposed model of MB and CV adsorption onto Zr_3O/AC, and similar observations were reported elsewhere [8]. From this study, the mechanism can be divided into these 4 fundamental steps:

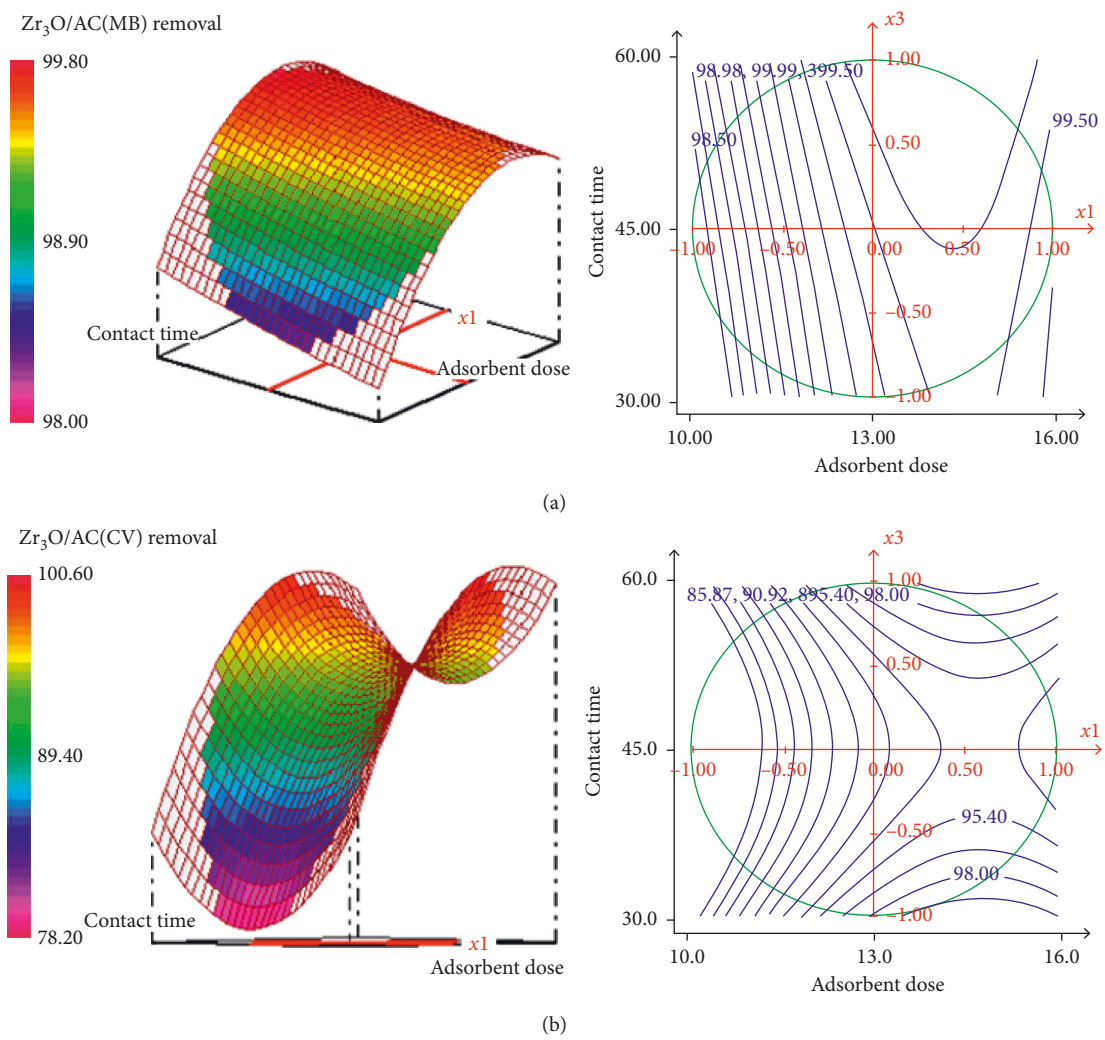

Figure 9: RSM and corresponding contour plot: (a) MB adsorption onto Zr_3O/AC as a function of adsorbent dose and contact time at the initial MB concentration constant; (b) CV adsorption onto Zr_3O/AC as a function of adsorbent dose and contact time at the initial MB concentration constant.

Table 8: Model validation.

Adsorbent dose = 12.66 mg V_m = 25 ml pH of solution, C_0 (MB) = 100 mg·L^{-1} W = 30 rpm T°C = 24 ± 1°C 58.08 min	Adsorption of MB (%) onto Zr_3O/AC	
	Predicted	Experimental
	99.60 ± 0.07	99.25
Adsorbent dose = 14.92 mg V_m = 25 ml pH of solution, C_0 (MB) = 100 mg·L^{-1} W = 30 rpm T°C = 24 ± 1°C 31.35 min	Adsorption of CV (%) onto Zr_3O/AC	
	Predicted	Experimental
	99.50 ± 0.22	99.01

(i) The adsorption of MB and CV molecules inside the Zr_3O/AC pores and the interaction between Zr-O and nitrogen of CV and MB

(ii) The hydrogen bonding would be produced between hydroxyl functional groups of Zr_3O/AC and the nitrogen of CV and MB

(iii) The π-π interaction between the double bonds of AC and molecule and that of pollutants

4. Conclusion

Zr_3O/AC was prepared by a facile chemical route and was characterized by different structural and textural techniques. The composite Zr_3O/AC was used as an efficient adsorbent for the MB and CV removal. Zr_3O/AC presented irregular particle size with a regular channel array and micro-mesopores. Also, numerous functional organic groups on the surface were observed by FTIR spectroscopy before and after MB and CV adsorption. Functional groups on the surface along with the porous structure, channel array, and physical interactions (π-π and hydrogen) between the

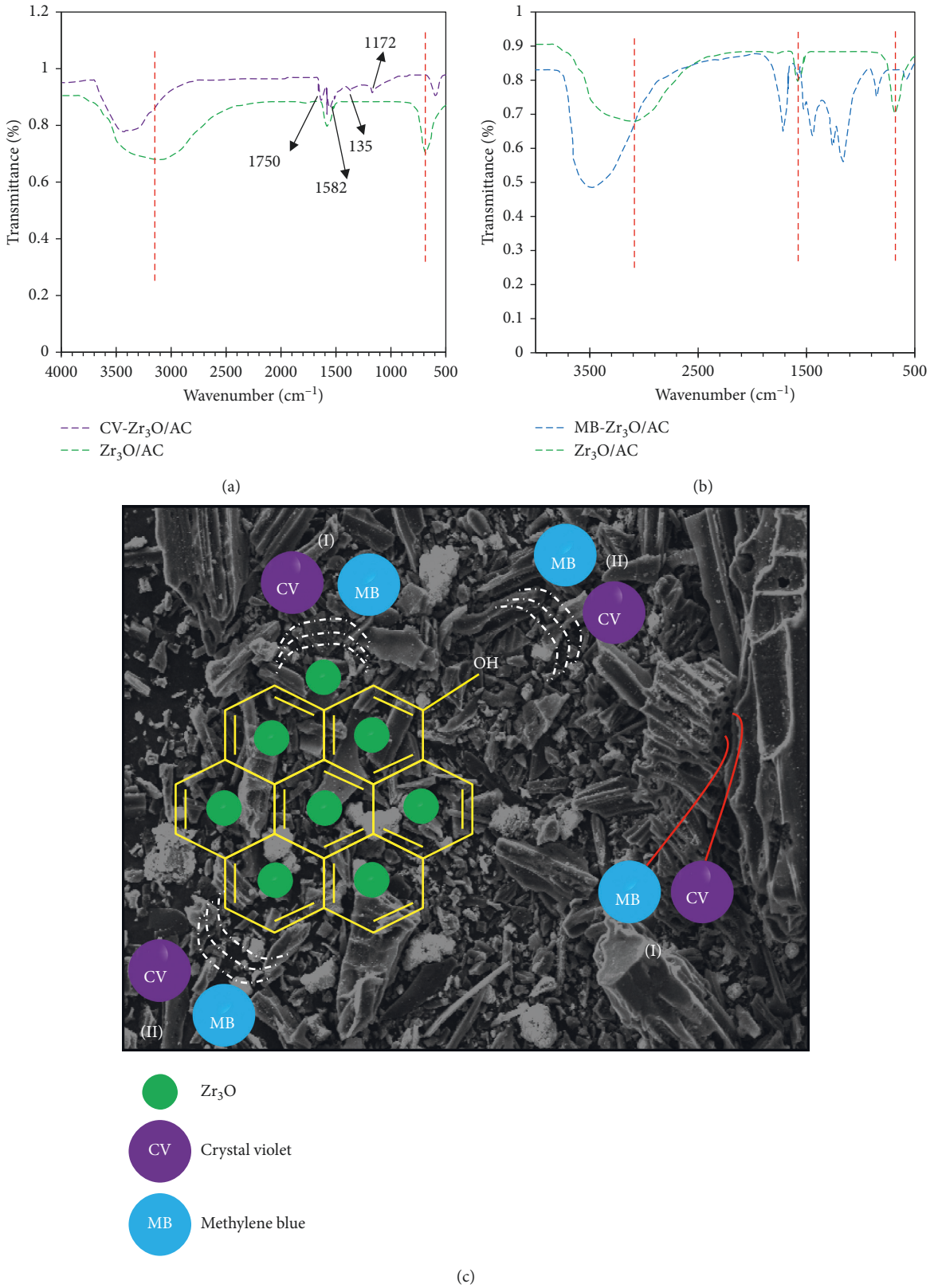

Figure 10: FTIR spectra of (a) Zr_3O/AC- and CV-loaded Zr_3O/AC, (b) Zr_3O/AC- and MB-loaded Zr_3O/AC, and (c) proposed adsorption mechanism.

Zr_3O/AC and the dyes are the main factors controlling the adsorption capacity. Langmuir and Freundlich models better described the adsorption process for MB and CV removal, respectively. The adsorption process followed the PSO kinetic model. Statistical response modeling together with the regression model helped us to optimize the experimental factors which provided a good fit with the experimental values.

Data Availability

Analysis data are available upon reasonable request to the corresponding author.

Conflicts of Interest

The authors declare that there no conflicts of interest regarding the publication of this paper.

Acknowledgments

The authors acknowledge the support of Ibn Zohr University and MASCIR Foundation for the support and help during SEM analyses.

Supplementary Materials

Supplementary material includes characterizations methods, response surface modeling procedure with a table reporting independent parameters, and response variables of the used matrix. Figures of linearized form of pseudo-second-order model, linearized form of Langmuir and Freundlich, and Pareto Chart were also reported in this section. (*Supplementary Materials*)

References

[1] F. Ansari, M. Ghaedi, M. Taghdiri, and A. Asfaram, "Application of ZnO nanorods loaded on activated carbon for ultrasonic assisted dyes removal: experimental design and derivative spectrophotometry method," *Ultrasonics Sonochemistry*, vol. 33, pp. 197–209, 2016.

[2] A. M. M. Vargas, A. L. Cazetta, M. H. Kunita, T. L. Silva, and V. C. Almeida, "Adsorption of methylene blue on activated carbon produced from flamboyant pods (*Delonix regia*): study of adsorption isotherms and kinetic models," *Chemical Engineering Journal*, vol. 168, no. 2, pp. 722–730, 2011.

[3] Y. Li, Q. Du, T. Liu et al., "Comparative study of methylene blue dye adsorption onto activated carbon, graphene oxide, and carbon nanotubes," *Chemical Engineering Research and Design*, vol. 91, no. 2, pp. 361–368, 2013.

[4] M. N. Ashiq, M. Najam-Ul-Haq, T. Amanat, A. Saba, A. M. Qureshi, and M. Nadeem, "Removal of methylene blue from aqueous solution using acid/base treated rice husk as an adsorbent," *Desalination and Water Treatment*, vol. 49, no. 1–3, pp. 376–383, 2012.

[5] Y. Ju, J. Fang, X. Liu et al., "Photodegradation of crystal violet in TiO_2 suspensions using UV–vis irradiation from two microwave-powered electrodeless discharge lamps (EDL-2): products, mechanism and feasibility," *Journal of Hazardous Materials*, vol. 185, no. 2-3, pp. 1489–1498, 2011.

[6] Y. Miyah, A. Lahrichi, M. Idrissi, S. Boujraf, H. Taouda, and F. Zerrouq, "Assessment of adsorption kinetics for removal potential of crystal violet dye from aqueous solutions using Moroccan pyrophyllite," *Journal of the Association of Arab Universities for Basic and Applied Sciences*, vol. 23, no. 1, pp. 20–28, 2017.

[7] H. Ait Ahsaine, M. Ezahri, A. Benlhachemi et al., "Novel Lu-doped Bi_2WO_6 nanosheets: synthesis, growth mechanisms and enhanced photocatalytic activity under UV-light irradiation," *Ceramics International*, vol. 42, no. 7, pp. 8552–8558, 2016.

[8] H. A. Ahsaine, M. Zbair, Z. Anfar et al., "Cationic dyes adsorption onto high surface area "almond shell" activated carbon: kinetics, equilibrium isotherms and surface statistical modeling," *Materials Today Chemistry*, vol. 8, pp. 121–132, 2018.

[9] I. Ali and V. K. Gupta, "Advances in water treatment by adsorption technology," *Nature Protocols*, vol. 1, no. 6, pp. 2661–2667, 2007.

[10] H. A. Ahsaine, M. Zbair, and R. El Haouti, "Mesoporous treated sewage sludge as outstanding low-cost adsorbent for cadmium removal," *Desalination and Water Treatment*, vol. 85, pp. 330–338, 2017.

[11] C.-Y. Cao, J. Qu, F. Wei, H. Liu, and W.-G. Song, "Superb adsorption capacity and mechanism of flowerlike magnesium oxide nanostructures for lead and cadmium ions," *ACS Applied Materials & Interfaces*, vol. 4, no. 8, pp. 4283–4287, 2012.

[12] S.-W. Nam, D.-J. Choi, S.-K. Kim, N. Her, and K.-D. Zoh, "Adsorption characteristics of selected hydrophilic and hydrophobic micropollutants in water using activated carbon," *Journal of Hazardous Materials*, vol. 270, pp. 144–152, 2014.

[13] V. Ranjithkumar, S. Sangeetha, and S. Vairam, "Synthesis of magnetic activated carbon/α-Fe_2O_3 nanocomposite and its application in the removal of acid yellow 17 dye from water," *Journal of Hazardous Materials*, vol. 273, pp. 127–135, 2014.

[14] E. Repo, J. K. Warchoł, A. Bhatnagar, and M. Sillanpää, "Heavy metals adsorption by novel EDTA-modified chitosan–silica hybrid materials," *Journal of Colloid and Interface Science*, vol. 358, no. 1, pp. 261–267, 2011.

[15] T. Zhai, S. Xie, X. Lu et al., "Porous $Pr(OH)_3$ nanostructures as high-efficiency adsorbents for dye removal," *Langmuir*, vol. 28, no. 30, pp. 11078–11085, 2012.

[16] Y. Zhang, Y. Li, L. Yang, X. Ma, L. Wang, and Z.-F. Ye, "Characterization and adsorption mechanism of Zn^{2+} removal by PVA/EDTA resin in polluted water," *Journal of Hazardous Materials*, vol. 178, no. 1–3, pp. 1046–1054, 2010.

[17] A. Hofmann, S. J. Clark, M. Oppel, and I. Hahndorf, "Hydrogen adsorption on the tetragonal ZrO_2(101) surface: a theoretical study of an important catalytic reactanty," *Physical Chemistry Chemical Physics*, vol. 4, no. 14, pp. 3500–3508, 2002.

[18] V. Hornebecq, C. Knöfel, P. Boulet, B. Kuchta, and P. L. Llewellyn, "Adsorption of carbon dioxide on mesoporous zirconia: microcalorimetric measurements, adsorption isotherm modeling, and density functional theory calculations," *Journal of Physical Chemistry C*, vol. 115, no. 20, pp. 10097–10103, 2011.

[19] A. Mullick and S. Neogi, "Acoustic cavitation induced synthesis of zirconium impregnated activated carbon for effective fluoride scavenging from water by adsorption," *Ultrasonics Sonochemistry*, vol. 45, pp. 65–77, 2018.

[20] W. Xiong, J. Tong, Z. Yang et al., "Adsorption of phosphate from aqueous solution using iron-zirconium modified activated carbon nanofiber: performance and mechanism,"

Journal of Colloid and Interface Science, vol. 493, pp. 17–23, 2017.

[21] S. Banerjee, S. R. Joshi, T. Mandal, and G. Halder, "Application of zirconium caged activated biochar alginate beads towards deionization of Cr(VI) laden water in a fixed bed column reactor," *Journal of Environmental Chemical Engineering*, vol. 6, no. 4, pp. 4018–4029, 2018.

[22] P. Suresh, J. J. Vijaya, and L. J. Kennedy, "Photocatalytic degradation of textile-dyeing wastewater by using a microwave combustion-synthesized zirconium oxide supported activated carbon," *Materials Science in Semiconductor Processing*, vol. 27, pp. 482–493, 2014.

[23] R. K. Prasad, "Degradation of biopolymeric pigments in distillery spentwash by electrocoagulation using copper anodes: statistical and canonical analysis," *Environmental Chemistry Letters*, vol. 8, no. 2, pp. 149–155, 2010.

[24] M. H. Kalavathy, I. Regupathi, M. Ganesa, and L. Rose, "Modelling, analysis and optimization of adsorption parameters for H_3PO_4 activated rubber wood sawdust using response surface methodology (RSM)," *Colloids and Surfaces B: Biointerfaces*, vol. 70, no. 1, pp. 35–45, 2009.

[25] J. N. Sahu, J. Acharya, and B. C. Meikap, "Response surface modeling and optimization of chromium(VI) removal from aqueous solution using Tamarind wood activated carbon in batch process," *Journal of Hazardous Materials*, vol. 172, no. 2-3, pp. 818–825, 2009.

[26] H. Yang, D. Zhou, Z. Chang, and L. Zhang, "Adsorption of crystal violet onto amino silica: optimization, equilibrium, and kinetic studies," *Desalination and Water Treatment*, vol. 52, no. 31–33, pp. 6113–6121, 2014.

[27] Z. Anfar, M. Zbair, H. A. Ahsaine, M. Ezahri, and N. El Alem, "Well-designed WO_3/activated carbon composite for Rhodamine B removal: synthesis, characterization, and modeling using response surface methodology," *Fullerenes, Nanotubes and Carbon Nanostructures*, vol. 26, no. 6, pp. 389–397, 2018.

[28] M. Zbair, H. Ait Ahsaine, and Z. Anfar, "Porous carbon by microwave assisted pyrolysis: an effective and low-cost adsorbent for sulfamethoxazole adsorption and optimization using response surface methodology," *Journal of Cleaner Production*, vol. 202, pp. 571–581, 2018.

[29] Z. Anfar, R. El Haouti, S. Lhanafi, M. Benafqir, Y. Azougarh, and N. El Alem, "Treated digested residue during anaerobic co-digestion of Agri-food organic waste: methylene blue adsorption, mechanism and CCD-RSM design," *Journal of Environmental Chemical Engineering*, vol. 5, no. 6, pp. 5857–5867, 2017.

[30] I. Langmuir, "The constitution and fundamental properties of solids and liquids. Part I. Solids," *Journal of the American Chemical Society*, vol. 38, no. 11, pp. 2221–2295, 1916.

[31] H. M. F. Freundlich, "Über die adsorption in lösungen," *Zeitschrift für Physikalische Chemie*, vol. 57A, pp. 385–470, 1906.

[32] M. Seredych, O. Mabayoje, M. M. Kolesnik, V. Krstic, and T. J. Bandosz, "Zinc (hydr)oxide/graphite based-phase composites: effect of the carbonaceous phase on surface properties and enhancement in electrical conductivity," *Journal of Materials Chemistry*, vol. 22, no. 16, pp. 7970–7978, 2012.

[33] Y. Sun, H. Li, G. Li, B. Gao, Q. Yue, and X. Li, "Characterization and ciprofloxacin adsorption properties of activated carbons prepared from biomass wastes by H_3PO_4 activation," *Bioresource Technology*, vol. 217, pp. 239–244, 2016.

[34] Y. Li, Q. Du, X. Wang et al., "Removal of lead from aqueous solution by activated carbon prepared from *Enteromorpha prolifera* by zinc chloride activation," *Journal of Hazardous Materials*, vol. 183, no. 1–3, pp. 583–589, 2010.

[35] S. Ghorai and K. K. Pant, "Equilibrium, kinetics and breakthrough studies for adsorption of fluoride on activated alumina," *Separation and Purification Technology*, vol. 42, no. 3, pp. 265–271, 2005.

[36] A. Sadezky, H. Muckenhuber, H. Grothe, R. Niessner, and U. Pöschl, "Raman microspectroscopy of soot and related carbonaceous materials: spectral analysis and structural information," *Carbon*, vol. 43, no. 8, pp. 1731–1742, 2005.

[37] W. Song, B. Gao, X. Xu et al., "Adsorption of nitrate from aqueous solution by magnetic amine-crosslinked biopolymer based corn stalk and its chemical regeneration property," *Journal of Hazardous Materials*, vol. 304, pp. 280–290, 2016.

[38] S. Vasudevan and J. Lakshmi, "The adsorption of phosphate by graphene from aqueous solution," *RSC Advances*, vol. 2, no. 12, pp. 5234–5242, 2012.

[39] S. Cheng, L. Zhang, H. Xia, and J. Peng, "Characterization and adsorption properties of La and Fe modified activated carbon for dye wastewater treatment," *Green Processing and Synthesis*, vol. 6, no. 5, p. 487, 2017.

[40] Z. Heidarinejad, O. Rahmanian, M. Fazlzadeh, and M. Heidari, "Enhancement of methylene blue adsorption onto activated carbon prepared from Date Press Cake by low frequency ultrasound," *Journal of Molecular Liquids*, vol. 264, pp. 591–599, 2018.

[41] M. E. Mahmoud, A. E. H. Abdou, and M. E. Sobhy, "Engineered nano-zirconium oxide-crosslinked-nanolayer of carboxymethyl cellulose for speciation and adsorptive removal of Cr(III) and Cr(VI)," *Powder Technology*, vol. 321, pp. 444–453, 2017.

[42] M. Zbair, Z. Anfar, H. Khallok, H. A. Ahsaine, M. Ezahri, and N. Elalem, "Adsorption kinetics and surface modeling of aqueous methylene blue onto activated carbonaceous wood sawdust," *Fullerenes, Nanotubes and Carbon Nanostructures*, vol. 26, no. 7, pp. 433–442, 2018.

[43] A. H. Jawad, R. A. Rashid, M. A. M. Ishak, and L. D. Wilson, "Adsorption of methylene blue onto activated carbon developed from biomass waste by H_2SO_4 activation: kinetic, equilibrium and thermodynamic studies," *Desalination and Water Treatment*, vol. 57, no. 52, pp. 25194–25206, 2016.

[44] G. Crini, H. N. Peindy, F. Gimbert, and C. Robert, "Removal of C.I. Basic Green 4 (Malachite Green) from aqueous solutions by adsorption using cyclodextrin-based adsorbent: kinetic and equilibrium studies," *Separation and Purification Technology*, vol. 53, no. 1, pp. 97–110, 2007.

[45] S. Lagergren, "Zur theorie der sogenannten adsorption geloester stoffe, kungliga svenska Vetenskapsakademiens," *Handlingar*, vol. 24, no. 4, pp. 1–39, 1898.

[46] Y. S. Ho and G. McKay, "Pseudo-second order model for sorption processes," *Process Biochemistry*, vol. 34, no. 5, pp. 451–465, 1999.

[47] W. J. Weber and J. C. Morris, "Intraparticule diffusion during the sorption of surfactants onto activated carbon," *Journal of Sanitary Engineering Division*, vol. 89, pp. 53–61, 1963.

[48] S. E. A. S. El-Deen and F.-S. Zhang, "Immobilisation of TiO_2-nanoparticles on sewage sludge and their adsorption for cadmium removal from aqueous solutions," *Journal of Experimental Nanoscience*, vol. 11, no. 4, pp. 239–258, 2016.

[49] Y. Chen, S. R. Zhai, N. Liu, Y. Song, Q. D. An, and X. W. Song, "Dye removal of activated carbons prepared from NaOH-pretreated rice husks by low-temperature solution-processed carbonization and H_3PO_4 activation," *Bioresource Technology*, vol. 144, pp. 401–409, 2013.

[50] M. A. Islam, S. Sabar, A. Benhouria, W. A. Khanday, M. Asif, and B. H. Hameed, "Nanoporous activated carbon prepared from karanj (*Pongamia pinnata*) fruit hulls for methylene blue adsorption," *Journal of the Taiwan Institute of Chemical Engineers*, vol. 74, pp. 96–104, 2017.

[51] O. Pezoti Junior, A. L. Cazetta, R. C. Gomes et al., "Synthesis of $ZnCl_2$-activated carbon from macadamia nut endocarp (*Macadamia integrifolia*) by microwave-assisted pyrolysis: optimization using RSM and methylene blue adsorption," *Journal of Analytical and Applied Pyrolysis*, vol. 105, pp. 166–176, 2014.

[52] T. Wang, S. Tan, and C. Liang, "Preparation and characterization of activated carbon from wood via microwave-induced $ZnCl_2$ activation," *Carbon*, vol. 47, no. 7, pp. 1880–1883, 2009.

[53] D. Pathania, S. Sharma, and P. Singh, "Removal of methylene blue by adsorption onto activated carbon developed from Ficus carica bast," *Arabian Journal of Chemistry*, vol. 10, pp. S1445–S1451, 2017.

[54] S. K. Ghosh, A. K. Hajra, and A. Bandyopadhyay, "Air agitated tapered bubble column adsorber for hazardous dye (crystal violet) removal onto activated ($ZnCl_2$) carbon prepared from bamboo leaves," *Journal of Molecular Liquids*, vol. 240, pp. 313–321, 2017.

[55] S. Senthilkumaar, P. Kalaamani, and C. Subburaam, "Liquid phase adsorption of crystal violet onto activated carbons derived from male flowers of coconut tree," *Journal of Hazardous Materials*, vol. 136, no. 3, pp. 800–808, 2006.

[56] C. A. Başar, "Applicability of the various adsorption models of three dyes adsorption onto activated carbon prepared waste apricot," *Journal of Hazardous Materials*, vol. 135, no. 1–3, pp. 232–241, 2006.

[57] T. Kannan, C. Buvaneswari, and N. Palvannan, "Removal of plant poisoning dyes by adsorption on Tomato Plant Root and green carbon from aqueous solution and its recovery," *Desalination*, vol. 249, no. 3, pp. 1132–1138, 2009.

[58] M. Zbair, Z. Anfar, H. A. Ahsaine, N. El Alem, and M. Ezahri, "Acridine orange adsorption by zinc oxide/almond shell activated carbon composite: operational factors, mechanism and performance optimization using central composite design and surface modeling," *Journal of Environmental Management*, vol. 206, pp. 383–397, 2018.

[59] S. Manna, D. Roy, P. Saha, D. Gopakumar, and S. Thomas, "Rapid methylene blue adsorption using modified lignocellulosic materials," *Process Safety and Environmental Protection*, vol. 107, pp. 346–356, 2017.

[60] B. Zhang, X. Han, P. Gu, S. Fang, and J. Bai, "Response surface methodology approach for optimization of ciprofloxacin adsorption using activated carbon derived from the residue of desilicated rice husk," *Journal of Molecular Liquids*, vol. 238, pp. 316–325, 2017.